Prediction of monoclinic single-layer Janus Ga_2TeX (X = S and Se): Strong in-plane anisotropy

M. Yagmurcukardes,[1,2,3,*] Y. Mogulkoc,[4] B. Akgenc,[5] A. Mogulkoc,[6] and F. M. Peeters[1]
[1]*Department of Physics, University of Antwerp, Groenenborgerlaan 171, B-2020 Antwerp, Belgium*
[2]*NANOlab Center of Excellence, Groenenborgerlaan 171, B-2020 Antwerp, Belgium*
[3]*Department of Photonics, Izmir Institute of Technology, 35430 Izmir, Turkey*
[4]*Department of Physics Engineering, Faculty of Engineering, Ankara University, 06100 Tandogan, Ankara, Turkey*
[5]*Department of Physics, Kirklareli University, Kirklareli, 39100, Turkey*
[6]*Department of Physics, Faculty of Sciences, Ankara University, 06100 Tandogan, Ankara, Turkey*

(Received 12 January 2021; revised 30 April 2021; accepted 21 June 2021; published 26 July 2021)

By using density functional theory (DFT) based first-principles calculations, electronic, vibrational, piezoelectric, and optical properties of monoclinic Janus single-layer Ga_2TeX (X = S or Se) are investigated. The dynamical, mechanical, and thermal stability of the proposed Janus single layers are verified by means of phonon bands, stiffness tensor, and quantum molecular dynamics simulations. The calculated vibrational spectrum reveals the either pure or coupled optical phonon branches arising from Ga-Te and Ga-X atoms. In addition to the in-plane anisotropy, single-layer Janus Ga_2TeX exhibits additional out-of-plane asymmetry, which leads to important consequences for its electronic and optical properties. Electronic band dispersions indicate the direct band-gap semiconducting nature of the constructed Janus structures with energy band gaps falling into visible spectrum. Moreover, while orientation-dependent linear-elastic properties of Janus single layers indicate their strong anisotropy, the calculated in-plane stiffness values reveal the ultrasoft nature of the structures. In addition, predicted piezoelectric coefficients show that while there is a strong in-plane anisotropy between piezoelectric constants along armchair (AC) and zigzag (ZZ) directions, there exists a tiny polarization along the out-of-plane direction as a result of the formation of Janus structure. The optical response to electromagnetic radiation has been also analyzed through density functional theory by considering the independent-particle approximation. Finally, the optical spectra of Janus Ga_2TeX structures is investigated and it showed a shift from the ultraviolet region to the visible region. The fact that the spectrum is between these regions will allow it to be used in solar energy and many nanoelectronics applications. The predicted monoclinic single-layer Janus Ga_2TeX are relevant for promising applications in optoelectronics, optical dichroism, and anisotropic nanoelasticity.

DOI: 10.1103/PhysRevB.104.045425

I. INTRODUCTION

Group-III monochalcogenides (MX, M = Ga, In; X = S, Se, Te), an important group of layered 2D materials exhibiting honeycomb lattice, possess intriguing electronic and optical properties. Monolayer MX crystals absorb light from visible to far-ultraviolet wavelengths ranging from 1.25 (IR) to 3.05 (UV), high photo current and the power conversion efficiency, hence they are alternative candidates in solar energy conversion [1,2], nanoelectronics [3,4], and optoelectronic applications [5–7]. To date, GaS [8,9], GaSe [10,11], GaTe [12], InSe [13,14], In_2Se_3 [15], and In_3Se_4 [16], important members of group-III chalcogenide monolayers, have been successfully synthesized and their properties have been extensively investigated [5,17–19].

Gallium telluride (GaTe) is one of the member of layered group-III monochalcogenides, which has been successfully synthesized in high quality by employing a facile chemical vapour deposition (CVD) technique [20]. It was demonstrated that the lattice orientation of grown GaTe can be effectively controlled by choosing suitable growth mode. Layered GaTe bulk crystal consists of weakly-interacting monoclinic GaTe layers having space group of C2/m with in-plane anisotropy. As a stable free-standing monolayer, GaTe is a semiconductor with an indirect band gap of 1.43 eV [21]. With its long-lifetime carriers, single-layer GaTe has been shown to exhibit remarkable photoresponsivity (above 10^4 A/W), which is two orders of magnitude higher than that of the MoS_2 photodetector [22], low-temperature micro-photoluminescence (PL) [23], short response time in photodetectors (around 6 ms) [20], and intense excitonic emission and absorption [24]. In addition, single-layer GaTe has been reported to be a promising candidate for thermoelectric devices [25], photocatalysis [2], phototransistors, photodetector, solar energy [26], and it has also been considered for detection of γ and x-ray radiation applications [27,28].

Recent experimental techniques have allowed researchers to controllably replace a complete layer of chalcogenide atom in single-layer MoX_2 (X = S or Se) in order to form a Janus structure with a complete out-of-plane asymmetry [29]. It was theoretically investigated that Janus structure exhibits an additional degree-of-freedom in piezoelectricity arising from the broken out-of-plane symmetry [30]. Following the

*mehmetyagmurcukardes.edu@gmail.com

synthesis of Janus MoSSe, Janus structures of various 2D single layers have been predicted by means of first-principles calculations [31–36]. Among the proposed Janus single layers, Ga_2SeTe and Ga_2SSe have been reported to exhibit direct band gaps of 0.90 and 1.21 eV, respectively, while Ga_2STe was shown to be an indirect band gap semiconductor with a band gap of 2.02 eV [37]. In addition, the optical absorption of the predicted Janus structures were shown to begin in the visible region with absorption coefficients larger than 10^4 cm^{-1}, which can be be used as ultraviolet detectors and photovoltaic absorbers. Moreover, single-layer Janus Ga_2SeTe was investigated to possess small effective mass of electron and hole, implying that the photogenerated carriers can be quickly transferred to the electrodes after absorption of photons. Thereby, Ga_2SeTe has been proposed as a new alternative candidate to be used in photovoltaic devices [38]. In another study, Kandemir *et al.* reported that in contrast to its analogs, Janus In_2SSe is a direct band-gap semiconductor, which is driven by the induced surface strain [39]. On the other hand, Zhou *et al.* reported that the piezoelectric performance of Janus group-III chalcogenide monolayers (Ga_2STe, Ga_2SeTe, In_2STe, and In_2SeTe) are up to four times higher than commonly used single-layer materials [40].

Notably, previous studies have been investigated and reported the in-plane isotropic, hexagonal structures of Janus M_2XY (M = Ga or In; X,Y = S, Se, or Te). However, it is known that GaTe possesses a layered bulk structure, which consists of stacked in-plane anisotropic monoclinic GaTe layers. Therefore, in this study, motivated by the stability of free-standing monoclinic GaTe single-layer, we have systematically investigated the stability of monoclinic Janus Ga_2TeSe and Ga_2TeS single layers. Our results revealed that both of the proposed structures exhibit dynamical and thermal stability and show significant anisotropy in their electronic, optical, and mechanical properties.

II. COMPUTATIONAL METHODOLOGY

For the first-principles calculations, the plane-wave basis projector augmented wave (PAW) method was employed in the framework of density functional theory (DFT) [41]. The generalized gradient approximation (GGA) in the Perdew-Burke-Ernzerhof (PBE)[42] form was used for the exchange-correlation potential as implemented in the Vienna *ab initio* simulation package (VASP) [43,44]. The kinetic energy cutoff for plane-wave expansion was set to 600 eV [45]. The van der Waals (vdW) interaction was included by using the DFT-D2 method [46]. The Brillouin zone (BZ) integration was performed by using a Γ-centered $16\times16\times1$ k-point mesh for the unit cell. The lattice constants and atoms were optimized without any constraint until the energy difference between two sequential steps were less than 10^{-5} eV, and maximum force on atoms was smaller than 10^{-3} eV $Å^{-1}$. The Gaussian smearing method was employed for the total-energy calculations and the width of the smearing was chosen as 0.05 eV. The vacuum space of ∼20 Å was inserted along the out-of-plane direction to avoid the unrealistic interactions between the repeating layers.

The electronic band dispersions were calculated within GGA and Heyd-Scuseria-Ernzerhof (HSE06) screened-nonlocal exchange functional [47]. The spin-orbit coupling (SOC) was also taken into account. The charge transfers between the individual atoms were calculated with decomposition of charge density into atomic contributions by applying Bader charge analysis technique [48].

Phonon band dispersions were calculated by using the small displacement method as implemented in the PHON code [49]. The phonon frequencies and the corresponding off-resonant Raman activities were calculated at the Γ point of the Brillouin zone (BZ) using the small displacement method. Each atom in the primitive unit cell was initially distorted by 0.01 Å and the corresponding dynamical matrix was constructed. Then, the vibrational modes were determined by a direct diagonalization of the dynamical matrix. The corresponding Raman activity of each phonon mode was obtained from the derivative of the macroscopic dielectric tensor by using the finite-difference method. The relaxed- and clamped-ion elastic stiffness tensors are calculated by using the small displacement methodology as implemented in VASP. In addition, the piezoelectric stress coefficients were directly obtained using density functional perturbation theory (DFPT) with a sufficiently large k-point sampling and kinetic-energy cutoff values.

The linear response of the system was described by the complex dielectric function, $\varepsilon(\omega) = \varepsilon_1(\omega) + i\varepsilon_2(\omega)$, where the Kramers-Kronig relation was applied to obtain the real and imaginary parts by using the PBE functional for optical calculations. Due to the exchange of Te-X atoms in the structures, the dipole correction was considered in order to remove effect of induced dipole.

Ab initio molecular dynamics (AIMD) simulations were carried out to examine the thermal stability of the 1T-distorted (1T′) structure of Ga_2TeX (X = Se, S) single layers by using 96 atoms at 300 K, 500 K, and 700 K with total simulation time of 6 ps. The time step was set to 2 fs and, to reach a total simulation time of 6 ps, 1000 steps were realized three times. Due to the large size of the cell, all the calculations were performed with each 2 ps [2 fs (1000 steps)]. Each 2 ps interval time step, the simulation was started again and continued to 6 ps. Starting from 300 K, the temperature was stepwise increased to 500 K and then 700 K within 6 ps total simulation time. As can be noticed from the snapshots taken at the considered temperatures, apart from minor distortions, the crystallinity of Ga2TeX (X = S and Se) monolayer is preserved, implying the stability even at high temperatures.

III. RESULTS

A. Structural and vibrational properties

In contrast to hexagonal S- and Se-based Ga-monochalcogenides, the most stable phase of GaTe exists in monoclinic structure. The layered monoclinic phase consists of weakly-stacked in-plane anisotropic GaTe layers. Single layer of GaTe is composed of two Ga atomic layers sandwiched between Te atoms possessing the C2/m space group with 2/m point group symmetry. Single-layer Janus structure is formed such that Te atoms on one surface of GaTe are replaced by S or Se atoms. In the simulated primitive unit cell of a Ga_2TeX (X = S or Se) layer, there

TABLE I. For the single-layer Janus Ga_2XTe structures, optimized in-plane lattice parameters, a and b; atomic bond lengths, d_{Ga-Ga}, d_{Ga-X}, and d_{Ga-Te}; donated amount of charge from Ga to X and Te atoms, $\Delta\rho_X$ and $\Delta\rho_{Te}$; cohesive energy per atom, E_{coh}; electronic band gaps calculated within PBE and HSE06, E_{gap}^{PBE} and E_{gap}^{HSE}; and valence/conduction band edge locations, VBM/CBM.

	a (Å)	b (Å)	d_{Ga-Ga} (Å)	d_{Ga-X} (Å)	d_{Ga-Te} (Å)	$\Delta\rho_X$ (e)	$\Delta\rho_{Te}$ (e)	E_{gap}^{PBE} eV	E_{gap}^{HSE} eV	VBM/CBM
Ga_2TeSe	22.45	3.92	2.42	2.46–2.51	2.66-2.70	0.6	0.4	1.64	2.40	Γ-Γ
Ga_2TeS	22.03	3.85	2.42	2.34–2.41	2.65-2.72	0.8	0.4	1.69	2.41	Γ-Γ

are 12 Ga and 12 chalcogenide atoms. The optimized in-plane lattice parameters reveal the in-plane anisotropy in both Janus single layers, Ga_2TeS and Ga_2TeSe. As listed in Table I, the lattice constants a–b are calculated to be 22.03–3.85 and 22.45–3.92 Å for single-layer Ga_2TeS and Ga_2TeSe, respectively. Two types of Ga-S and Ga-Te bonds are found to be formed in single-layer Ga_2TeS. The short and long Ga-S bond lengths are found to be 2.34 and 2.41 Å while those of Ga-Te are 2.65 and 2.72 Å, which indicates the formation of surface strain on the S-side of the Janus single layer. In the case of single-layer Ga_2TeSe, the Ga-Se bonds are 2.46 and 2.51 Å while Ga-Te bonds on the Te-side are found as 2.66 and 2.70 Å, respectively. In addition, the charge-density difference shown in the bottom panel of Fig. 1(a) indicates the charge asymmetry on the Janus surfaces.

The dynamical stability of both Janus structures are predicted by calculating the phonon band dispersions through the whole BZ. As presented in the Figs. 1(b) and 1(c), Janus single layers, Ga_2TeSe and Ga_2TeS, are free from any imaginary frequencies through the whole BZ, indicating their dynamical stability. The phonon band dispersions show that the out-of-plane acoustical phonon branch (ZA) has a very low dispersion in each single layer around the Γ and Y points. The extremely low dispersion of ZA branch indicates that the constant volume heat capacities of the materials scales with temperature with higher powers. In addition, those low-dispersive branches reveal the high thermal conductivity of the predicted single layers. It was reported in 2D materials that as the quadratic behavior of ZA branch approaches to linear dispersion, the thermal conductivity decreases [50]. Each single-layer structure is found to exhibit 69 optical phonon branches out of the three acoustical phonons. Note that due to anisotropy of the crystal structure, all the optical phonon branches are non-degenerate. The highest phonon frequencies at the Γ point of the BZ reveal the quite stronger Ga-S bonds as compared to Ga-Se bond formations. For the stable Janus single layers, Ga_2TeSe and Ga_2TeS, we also calculated the Raman activity of each optical-phonon branch at the Γ point [Fig. 2(a)]. The phonon modes labeled from I-to-VI represent the most prominent Raman active modes. In the Fig. 2(b), the mode I represents the mostly in-plane vibrations of Ga-S/Se atoms while the phonon mode II arises from the mixed vibration of Ga-Te-X atoms dominated by the out-plane vibrations. For the relatively low-frequency phonon modes, namely from II-to-VI, Te atoms have also contributions to the atomic vibrations. Apparently, the Raman spectra are key analysis for the determination of crystal structure of the predicted Janus single layers. In addition, the atomic vibrations indicated above can be used to identify the Janus formation since the different atomic types on different surfaces show distinctive features. For instance as mentioned above, while some Raman active modes are dominated only by one type of surface atoms, some phonon modes possess coupled vibrations of all atoms.

B. Mechanical and thermal stability

Apart from the dynamical stability of the Janus single layers, the mechanical stability of each structure is also examined by calculating their elastic-stiffness tensors. Firstly, it is found that the predicted Janus single layers Ga_2TeS and Ga_2TeSe are mechanically stable structures that the calculated elastic-tensor elements obey the Born criteria, $C_{11}C_{22} > C_{21}^2$. For the mechanically stable Janus structures, the orientation-dependent elastic parameters are calculated in order to investigate the linear-elastic properties.

The two independent elastic constants: The in-plane stiffness (C) and Poisson ratio (ν) are expected to exhibit orientation dependency arising from the monoclinic symmetry. In order to determine in-plane anisotropy in the elastic constants, the elastic-strain tensor elements (C_{ij}) are obtained and the corresponding C and ν values are obtained in for all orientations of the lattice using the formulas:

$$C(\theta) = \frac{\left(C_{11}C_{22} - C_{12}^2\right)}{C_{22}\cos^4(\theta) + A\cos^2(\theta)\sin^2(\theta) + C_{11}\sin^4(\theta)}, \quad (1)$$

$$\nu(\theta) = \frac{C_{12}\cos^4(\theta) - B\cos^2(\theta)\sin^2(\theta) + C_{12}\sin^4(\theta)}{C_{22}\cos^4(\theta) + A\cos^2(\theta)\sin^2(\theta) + C_{11}\sin^4(\theta)}, \quad (2)$$

where the numbers A and B are defined as $A = (C_{11}C_{22} - C_{12}^2)/C_{66} - 2C_{12}$ and $B = C_{11} + C_{22} - (C_{11}C_{22} - C_{12}^2)/C_{66}$. The angle θ as the angle of orientation measured from the AC direction in counterclockwise.

The in-plane stiffness, which is known to be the measure of the rigidity of a 2D material, is calculated to be 51 and 58 N/m for the AC and ZZ orientations, respectively, for single-layer Ga_2TeS while two values are found to be 44 and 57 N/m for Ga_2TeSe. Apparently, the stiffness along the AC direction smaller than that of ZZ direction. This is a direct consequence of the quasi-1D nature of the crystal lattice. In other words, the atomic bonds are quite stronger along the ZZ direction. Similar anisotropy is found for the Poisson ratio, which is defined as the ratio of the transverse contraction strain to the longitudinal extension, as presented in Fig. 3(b). Along the two main orientations, AC/ZZ, the Poisson ratio values are found to be 0.26/0.30 and 0.22/0.28 for single-layer Ga_2TeS and Ga_2TeSe, respectively. The calculated elastic constants, overall, reveal the soft nature of the predicted Janus single layers. As shown in Fig. 3(b), the Poisson ratio values are all positive for all orientations of the predicted Janus structures

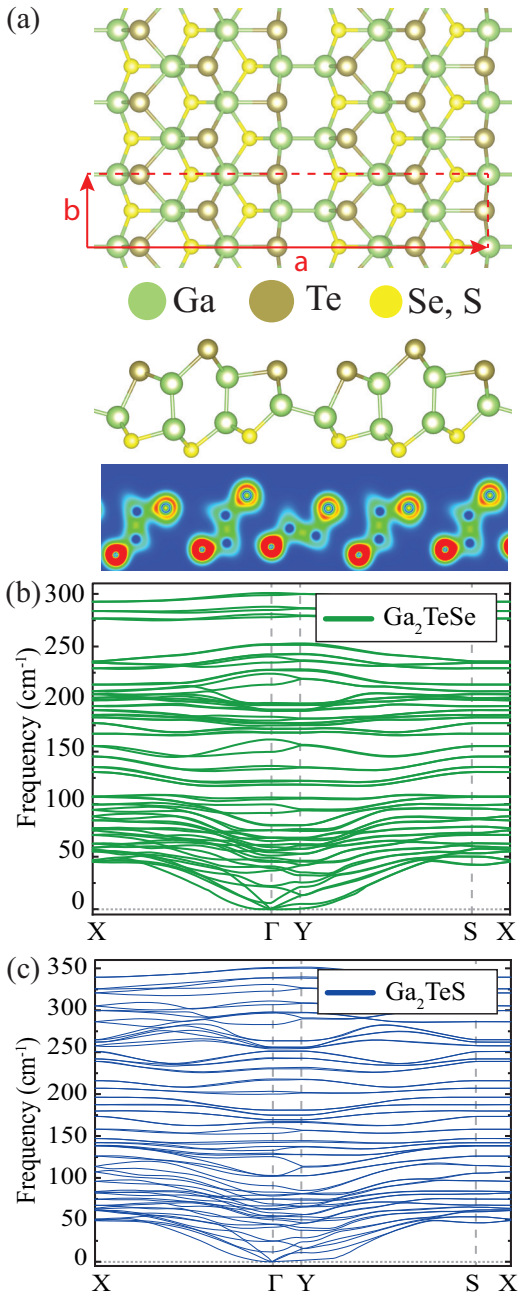

FIG. 1. For the Janus single layers of Ga_2TeSe and Ga_2TeS; (a) top and side views and the corresponding charge distribution on the individual atoms. [(b), (c)] The phonon band dispersions for Ga_2TeSe and Ga_2TeS, respectively. The primitive unit cell is denoted by the red lines by representing the lattice vectors, a and b. The blue regions represent the zero charge regime while the yellow regions stand for the charge of 6.4 $e/Å^3$. The green region represents the charge amount of 1.9 $e/Å^3$ while the maximum charge region, red region, shows the 6.9 $e/Å^3$.

indicating nonauxetic behavior of the crystals. As reported in the literature, the auxetic behavior in 2D materials can be obtained in materials exhibiting puckered structures [51]. The auxetic behavior indicates the stretching of a material in a direction when stretched along the perpendicular direction in contrast to most of the materials having positive Poisson ratio. In our predicted Janus structures, however, the auxetic behavior is not present.

In addition, the thermal stability are examined by performing *ab initio* molecular dynamics (AIMD) simulations using NVT ensemble with fixed particle number, volume, and temperature and our results are presented in the Supplemental Material (SM) [52]. For the AIMD simulations, 32-atom supercell is used for each single layer with a k-mesh of $4\times4\times1$. The dynamical investigations are started with the optimized structure of the 1T-distorted (1T′) structure of Ga_2TeX (X = Se, S) single layers at 0 K. Starting from 300 K, the temperature is stepwise increased to 500 K and then 700 K within 6 ps total simulation time. The evolution of free energy for Ga_2TeX (X = Se, S) atomic structures during the simulation time is shown in Figs. S1 and S2 within the SM [52]. The time step was set to 2 fs (1000 steps) with a total simulation time of 6 ps. The structure snapshots are taken at the end of the each simulation in every 2 ps. As can be noticed from the snapshots taken at the considered temperatures, apart from minor distortions, the crystallinity of Ga_2TeX (X = Se, S) atomic structures is preserved, implying the stability even at high temperatures.

C. Piezoelectric properties

Piezoelectricity is known as the generation of electric dipole moment as a result of external mechanical stress occurring in noncentrosymmetric materials. In the case of 2D materials, it was reported that single layers of TMDs exhibit intrinsic in-plane piezoelectric properties [53] while the buckled single-layer forms of group-IV monochacogenides were shown to possess out-of-plane piezoelectricity arising from their buckled asymmetric structures [54]. The relaxed-ion piezoelectric tensor elements e_{ij} are described as the sum of ionic and the electronic contributions. And the piezoelectric stress tensor is related to the piezoelectric strain tensor, denoted as d_{ij}, using the elastic stiffness tensor elements C_{ij} by the equation

$$e_{ij} = d_{ik}C_{kj}. \tag{3}$$

Our results for the tetragonal phase of Janus Ga_2XTe reveal that there exist five nonzero elements of e_{ij}, which are e_{11}, e_{12}, e_{24}, e_{31}, and e_{32} constants exhibiting in-plane anisotropy. Therefore, driving the equation above for the nonzero elements we have the following relations:

$$d_{11} = \frac{e_{11}C_{22} - e_{12}C_{21}}{C_{11}C_{22} - C_{12}C_{21}}, \tag{4}$$

$$d_{12} = \frac{e_{12}C_{11} - e_{11}C_{12}}{C_{11}C_{22} - C_{12}C_{21}}, \tag{5}$$

$$d_{24} = \frac{e_{24}}{C_{44}}, \tag{6}$$

$$d_{31} = \frac{e_{31}C_{22} - e_{32}C_{21}}{C_{11}C_{22} - C_{12}C_{21}}, \tag{7}$$

$$d_{32} = \frac{e_{32}C_{11} - e_{31}C_{12}}{C_{11}C_{22} - C_{12}C_{21}}. \tag{8}$$

As given in the Eqs. (4)–(8), the nonzero coefficients e_{11} and e_{12} represent the induced polarizations along the AC and ZZ directions, respectively when the strain is applied along

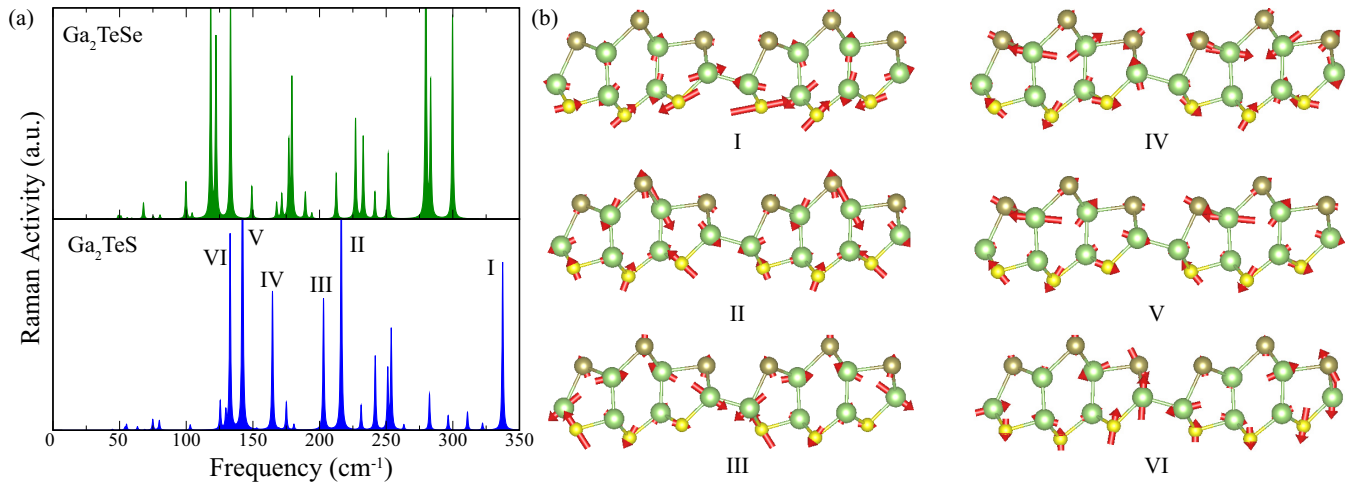

FIG. 2. (a) Raman spectra of Janus single layers Ga_2TeSe and Ga_2TeS. (b) The atomic vibrations in some of the prominent Raman active modes.

AC direction. On the other hand, e_{31} and e_{32} stand for the induced polarizations along the AC and ZZ directions when the strain is applied vertically, i.e., along z direction. In addition, the coefficient e_{24} specifically represents the induced polarization along both AC and ZZ directions when the strain is applied along the ZZ direction.

As listed in Table II, there is an in-plane anisotropy between the piezoelectric coefficients when the strain is applied along either AC or out-of-plane directions. When an external electric field is applied along the AC direction, the induced stress in the structures along AC and ZZ directions are different. The calculated d_{11}/d_{12} values are 1.36/–2.89 and 1.75/–4.23 pm/V for single layers of Ga_2TeSe and Ga_2TeS, respectively. The minus sign for the ZZ direction means that as the field is applied, the structures get compressed along ZZ direction. Similarly, both single layers exhibit negative response along AC and ZZ directions when the field is applied along ZZ direction (d_{24} values are –3.26 and –4.51 pm/V for Ga_2TeSe and Ga_2TeS, respectively). The formation of Janus single layers creates the piezoelectricity in the AC and ZZ directions when the external field is applied along the out-of-plane direction. However, it should be noted that when the field is applied along the out-of-plane direction, the induced strain along AC direction in both single layers is negligibly small. In contrast, the induced strain along ZZ direction is considerable (0.23 and 0.34 pm/V for Ga_2TeSe and Ga_2TeS, respectively).

We also mention about the net dipole moments occurring in the Janus single layers predicted in the present paper. The net dipole moments along three main directions, namely x, y, and z directions, are calculated in unit of eÅ. The net dipole moments along the in-plane directions, x/y, are calculated to be 17.8/88.6 eÅ and 14.8/86.8 eÅ for single layers of Ga_2TeSe and Ga_2TeS, respectively. The formation of Janus structures results in the creation of net dipole moments along the out-of-plane directions (0.3 and 0.4 eÅ for Ga_2TeSe and Ga_2TeS, respectively). Apparently, the dipole moments along the out-of-plane direction is very weak as compared to those

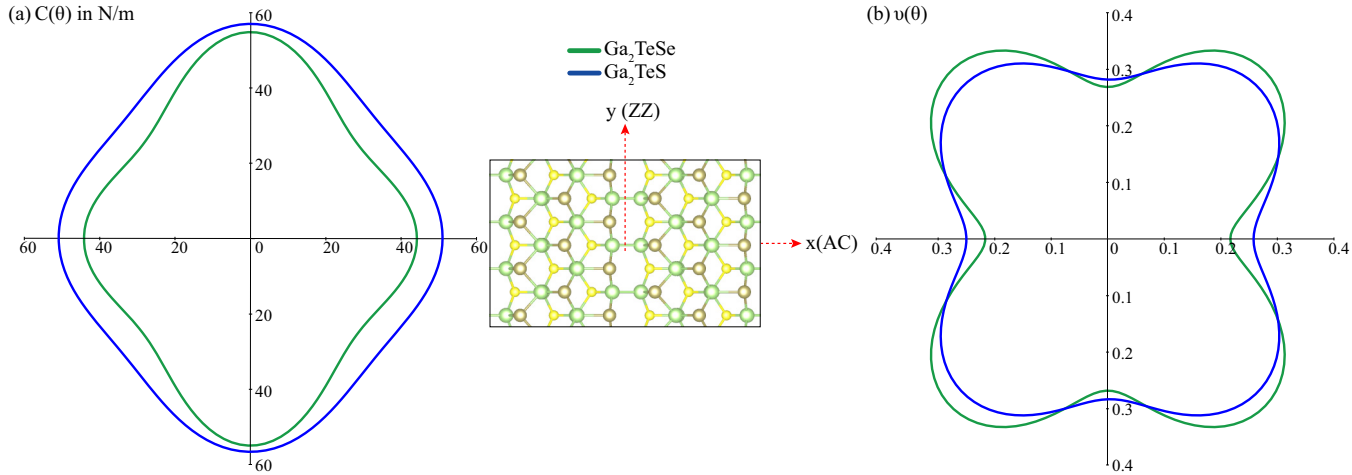

FIG. 3. Orientation-dependent linear-elastic constants for Ga_2TeX, (a) in-plane stiffness and (b) Poisson ratio. The two main orientations, namely x (AC) and y (ZZ), are shown on the crystal structure. The blue and green curves stand for single layers Ga_2Tes and Ga_2TeSe, respectively.

TABLE II. For the single-layer Janus Ga_2XTe structures, the elastic stiffness tensor elements, C_{11}, $C_{21} = C_{12}$, and C_{22}; the relaxed-ion piezoelectric stress coefficients, e_{11}, e_{12}, e_{24}, e_{31}, and e_{32}; and the piezoelectric strain coefficients, d_{11}, d_{12}, d_{24}, d_{31}, and d_{32}. Note that the unit of e_{ij} is given in $\times 10^{-10}$ C/m while that of d_{ij} is given in pm/V.

	C_{11} (N/m)	C_{21} (N/m)	C_{22} (N/m)	e_{11} (C/m)	e_{12} (C/m)	e_{24} (C/m)	e_{31} (C/m)	e_{32} (C/m)	d_{11} (pm/V)	d_{12} (pm/V)	d_{24} (pm/V)	d_{31} (pm/V)	d_{32} (pm/V)
Ga_2TeSe	47	13	60	0.26	–1.56	–0.45	0.03	0.14	1.36	–2.89	–3.26		0.23
Ga_2TeS	55	16	63	0.27	–2.36	–0.75	0.05	0.21	1.75	–4.23	–4.51	0.05	0.34

along in-plane directions as a result of the 2D nature of the structures. In order to compare our results with those reported in the literature for other 2D materials, the polarizations are calculated using the net dipole moments given above. Note that the polarization is given as the dipole moment per unit area in 2D structures. Our calculated in-plane polarizations for the x/y directions are 324/1611 and 279/1634 pC/m for Ga_2TeSe and Ga_2TeS, respectively. The values along the x direction are lower than those reported for single layers of GeSe (357 pC/m) and GeS (484 pC/m) while greater than those reported for SnS (260 pC/m) and SnSe (181 pC/m) [55]. Moreover, the induced out-of-plane polarizations for single-layer Ga_2TeSe and Ga_2TeS are calculated to be 7×10^{-3} and 9×10^{-3} C/m^2 assuming an effective thickness of approximately 8 Å for each single layer. As compared to the out-of-plane polarization of GeSe (1.9 C/m^2) [56], our results for the Janus single layers of Ga_2TeSe and Ga_2TeS are much smaller due to the weak out-of-plane dipoles.

D. Electronic and optical properties

The projected band structure of Ga_2TeX with the different atomic contribution is shown in Fig. 4 in the framework of DFT-PBE. It is clear that both structures predict an direct band-gap semiconductors with an energy band gap of 1.64 eV (1.69 eV) for Ga_2TeS (Ga_2TeSe) between the valence-band maximum (VBM) and the conduction-band minimum (CBM) at the Γ point of BZ. It is obvious from the Fig. 4 that the VBM is dominated by the Te atom for the both structures. However, the main contribution to the CBM comes from Ga atom and the S and Se atoms contribute insignificantly around the vicinity of VBM and CBM of the band structures. To get better understanding about electronic structure, effect of spin-orbit coupling and hybrid functional are considered on top of the PBE approach. The inclusion of spin-orbit coupling decreases the band gap and it becomes 1.54 eV (1.61 eV) for Ga_2TeS (Ga_2TeSe) as shown in Fig. 5. Moreover, the hybrid functionals (HSE06) are taking into account to get more accurate electronic structure. The resulting band structures with HSE06 have the same character, only the band gap increases to 2.40 eV (2.41 eV) for Ga_2TeS (Ga_2TeSe) due to the shifting of the conduction bands to the higher energy values.

The investigation of the optical properties of materials are effective in particular to envision the industrial applications. The optical response of Ga_2TeX is analyzed by calculating the imaginary part of the dielectric function $\varepsilon_2(\omega)$, which is presented in Figs. 6 and 7. The total equation for this function is demonstrated below:

$$\varepsilon^{(2)}_{\alpha\beta}(\omega) = \frac{4\pi^2 e^2}{\Omega} \lim_{q\to 0} \frac{1}{q^2} \sum_{c,v,\boldsymbol{k}} 2\omega_{\boldsymbol{k}} \delta(\epsilon_{c\boldsymbol{k}} - \epsilon_{v\boldsymbol{k}} - \omega) \times \langle u_{c+\boldsymbol{k}+\boldsymbol{e}_{\alpha q}} | u_{v\boldsymbol{k}} \rangle \langle u_{c+\boldsymbol{k}+\boldsymbol{e}_{\beta q}} | u_{v\boldsymbol{k}} \rangle^*, \quad (9)$$

where the c and v correspond to conduction and valence band states, respectively, and $u_{c\mathbf{k}}$ is the cell periodic part of the orbitals at the k-point $\mathbf{k}$.

The variation of imaginary part of the dielectric function for Ga_2TeX versus the energy of the incident photon (in eV) is illustrated in Figs. 6 and 7 with respect to x and y directions for Ga_2TeS and Ga_2TeSe single layers. We have performed the exhaustive characterization of optical properties (i.e., absorption, reflectivity, and conductivity) of Ga_2TeX in Fig. 6. The imaginary part of dielectric function onsets of the structures

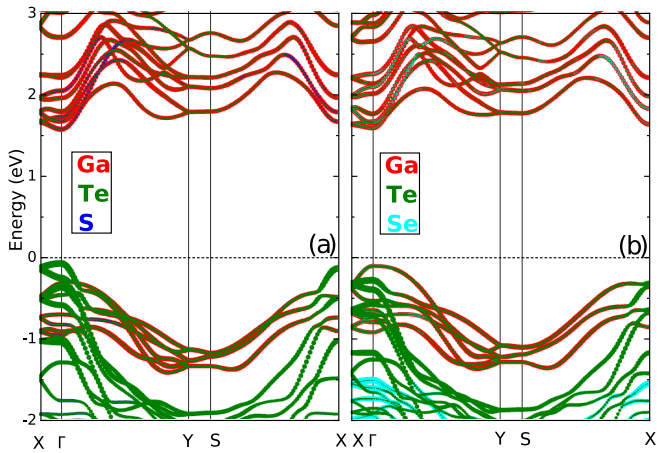

FIG. 4. The atom-dependent projected electronic band structures for (a) Ga_2TeS and (b) Ga_2TeSe in the scheme of DFT-PBE.

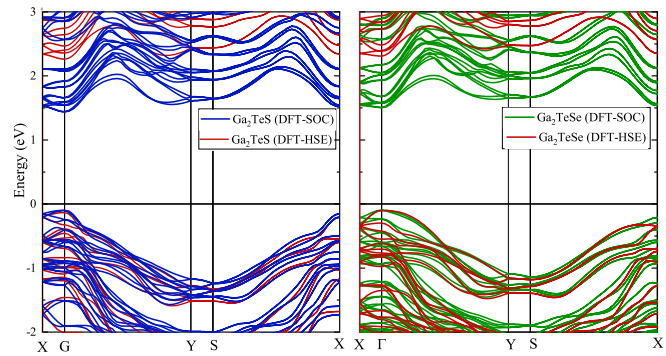

FIG. 5. The electronic band structure of Ga_2TeX in the framework of DFT-SOC and HSE06.

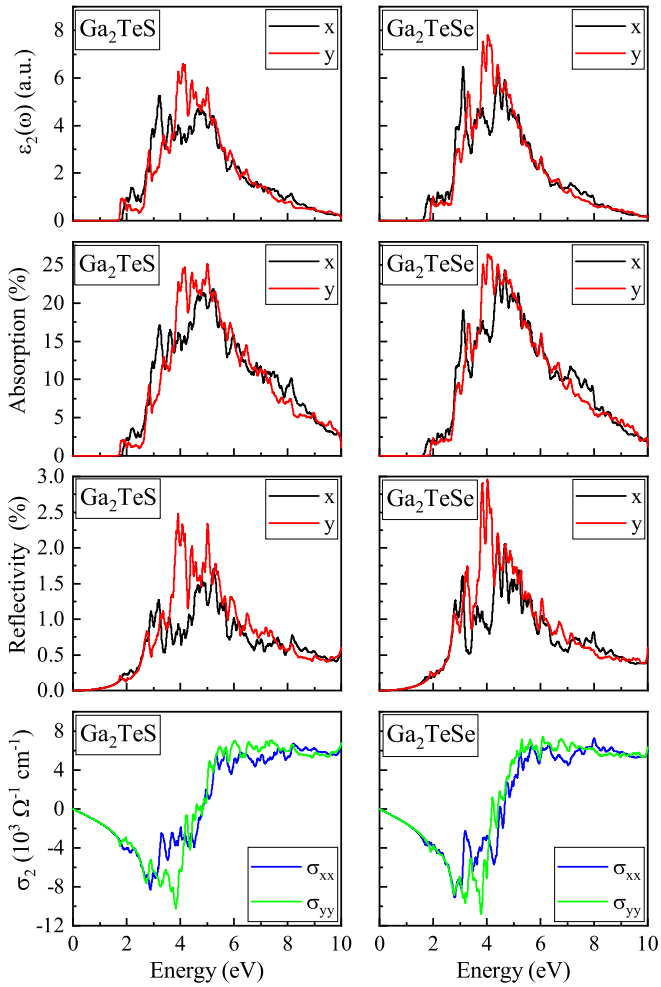

FIG. 6. For single layers of Ga_2TeS (left panel) and Ga_2TeSe (right panel); [(a), (b)] imaginary part of the dielectric function, [(c), (d)] absorption, [(e), (f)] reflectivity, and [(g), (h)] directional optical conductivity.

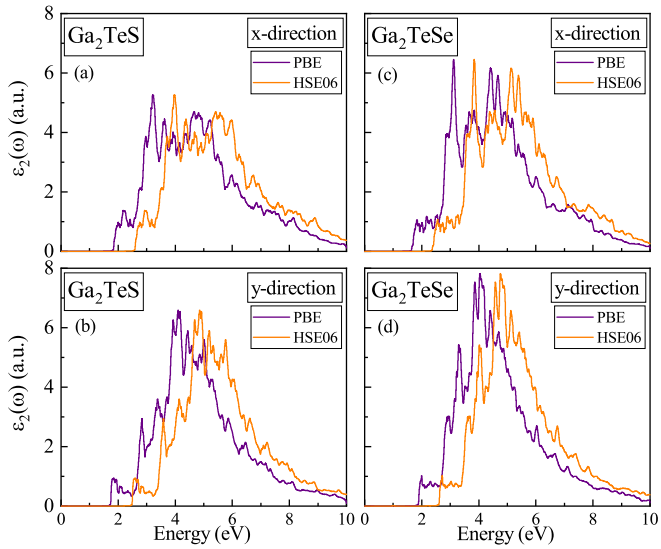

FIG. 7. The variation of the imaginary part of the dielectric function of with photon energy for in-plane polarization for Ga_2TeX calculated within PBE and HSE06 functionals.

are compatible with their energy band gaps as presented in Fig. 5. Optical calculations were repeated at different vacuum values and it was observed that the intensity of the dielectric function changed as the vacuum values changed, the onsets remained the same and exhibited in Fig. S3 (see SM [52]). The properties of the optical spectrum can be observed in the x and y directions due to the presence of anisotropy. The main peak region of absorption of Ga_2TeX generally along x and y directions center around 3 eV and 4 eV, respectively. Considering the HSE06 values, high efficiency is expected since the strong absorption, which means high efficiency in solar energy use, is observed along the y direction from ultraviolet (UV) to the visible light region. The absorption intensity along the x direction is lower than along the y direction in the visible light region for all Ga_2TeX structures. However, the very strong main peak along y direction of Ga_2TeSe is observed around 4 eV, which is higher than that Ga_2TeS x and y directions. The local field effects are ignored due the much more computational costs. Due to the frequency-dependent reflection, it is seen that the reflection in the visible and UV spectrum is in both directions. This allows the material to be used in optoelectronic devices. We also examine the optical conductivity for in-plane polarization of light. As evident in Fig. 6, σ_{xx} and σ_{yy} are in the low-energy regime until 5 eV, indicating that the system is transparent in the infrared and visible regions. Further to the onset around 2.5 eV, σ_{xx} displays an abrupt increase in absorption beyond 5.5 eV in the UV region while σ_{yy} of the Ga_2TeS structure has minimum around 4 eV. The variation of $\varepsilon_2(\omega)$ with photon energy for in-plane light polarization is given in Fig. 7. Based on HSE06 results (as is seen from the figure HSE06 band gaps have larger values than PBE), for Ga_2TeX structures the onset of absorption generally are at 2 eV in accordance with the direct electronic band gap, and main absorption peaks have mostly extended to UV region.

IV. CONCLUSION

In the present paper, density functional theory-based first principles calculations were performed in order examine the dynamical and thermal stability of monoclinic Janus single layers of Ga_2TeS and Ga_2TeSe. For the stable single-layer structures, vibrational, electronic, optical, mechanical properties were investigated in terms of the anisotropy in the crystal. Raman spectra analysis revealed the existence of either pure or coupled phononic vibrations arising from Ga-Te-X (X = S or Se) atoms. Electronic band dispersions calculations indicated the direct band-gap nature of the predicted Janus single layers whose energy band gaps were calculated to be in the visible spectrum. Elastically, Ga_2TeS and Ga_2TeSe Janus structures, which exhibit in-plane anisotropy due to their quasi 1D nature, were shown to be quite soft as compared to well-known 2D materials. Moreover, predicted piezoelectric coefficients revealed that while there is a strong in-plane anisotropy between piezoelectric constants along AC and ZZ directions, there exists a tiny polarization along the out-of-plane direction as a result of the formation of Janus structure. The optical dichorism and three-fold anisotropy of the proposed Janus single layers make them potential candidates for promising applications. The optical spectra of Ga_2TeS and Ga_2TeSe

Janus structures were similar to group-III chalcogenide monolayers. It was in the form of transition from ultraviolet to visible region.

ACKNOWLEDGMENTS

Computational resources were provided by TUBITAK ULAKBIM, High Performance and Grid Computing Center (TR-Grid e-Infrastructure) and by Flemish Supercomputer Center (VSC). B.A. acknowledges financial support from the Kırklareli University-BAP under Project No. 201. Y.M. and A.M. acknowledge the Ankara University for high performance computing facility through the AYP under Grant No. 17A0443001. M.Y. was supported by the Flemish Science Foundation (FWO-Vl) as a postdoctoral fellowship.

[1] J. Wang, H. Guo, J. Xue, D. Chen, G. Yang, B. Liu, H. Lu, R. Zhang, and Y. Zheng, Solar RRL **3**, 1900321 (2019).
[2] S. S. A. Al-Abbas, M. K. Muhsin, and H. R. Jappor, Chem. Phys. Lett. **713**, 46 (2018).
[3] H. R. Jappor, Physica B: Condens. Matter. **524**, 109 (2017).
[4] Y. Shao, Q. Wang, H. Pan, and X. Shi, Adv. Electron. Mater. **6**, 1900981 (2020).
[5] H. R. Jappor, M. M. Obeid, T. V. Vu, D. Hoat, H. D. Bui, N. N. Hieu, S. J. Edrees, Y. Mogulkoc, and R. Khenata, Superlattice Microst. **130**, 545 (2019).
[6] H. R. Jappor and M. A. Habeeb, Phys. E: Low Dimens. Syst. Nanostruct. **101**, 251 (2018).
[7] H. L. Zhuang and R. G. Hennig, Chem. Mater. **25**, 3232 (2013).
[8] S. Yang, Y. Li, X. Wang, N. Huo, J.-B. Xia, S.-S. Li, and J. Li, Nanoscale **6**, 2582 (2014).
[9] A. Harvey, C. Backes, Z. Gholamvand, D. Hanlon, D. McAteer, H. C. Nerl, E. McGuire, A. Seral-Ascaso, Q. M. Ramasse, N. McEvoy *et al.*, Chem. Mater. **27**, 3483 (2015).
[10] P. Hu, Z. Wen, L. Wang, P. Tan, and K. Xiao, ACS nano **6**, 5988 (2012).
[11] S. Lei, L. Ge, Z. Liu, S. Najmaei, G. Shi, G. You, J. Lou, R. Vajtai, and P. M. Ajayan, Nano Lett. **13**, 2777 (2013).
[12] Z. Wang, K. Xu, Y. Li, X. Zhan, M. Safdar, Q. Wang, F. Wang, and J. He, ACS Nano **8**, 4859 (2014).
[13] W. Feng, X. Zhou, W. Q. Tian, W. Zheng, and P. Hu, Phys. Chem. Chem. Phys. **17**, 3653 (2015).
[14] M. Wu, J.-J. Shi, M. Zhang, Y.-m. Ding, H. Wang, Y.-L. Cen, and J. Lu, Nanoscale **10**, 11441 (2018).
[15] J. O. Island, S. I. Blanter, M. Buscema, H. S. van der Zant, and A. Castellanos-Gomez, Nano Lett. **15**, 7853 (2015).
[16] G. Han, Z.-G. Chen, C. Sun, L. Yang, L. Cheng, Z. Li, W. Lu, Z. M. Gibbs, G. J. Snyder, K. Jack *et al.*, Cryst. Eng. Commun. **16**, 393 (2014).
[17] Z. Yang and J. Hao, Adv. Mater. Technol. **4**, 1900108 (2019).
[18] M. Yagmurcukardes, C. Sevik, and F. M. Peeters, Phys. Rev. B **100**, 045415 (2019).
[19] M. Demirtas, B. Ozdemir, Y. Mogulkoc, and E. Durgun, Phys. Rev. B **101**, 075423 (2020).
[20] Z. Wang, M. Safdar, M. Mirza, K. Xu, Q. Wang, Y. Huang, F. Wang, X. Zhan, and J. He, Nanoscale **7**, 7252 (2015).
[21] S. Demirci, N. Avazli, E. Durgun, and S. Cahangirov, Phys. Rev. B **95**, 115409 (2017).
[22] F. Liu, H. Shimotani, H. Shang, T. Kanagasekaran, V. Zolyomi, N. Drummond, V. I. Fal'ko, and K. Tanigaki, ACS Nano **8**, 752 (2014).
[23] O. Del Pozo-Zamudio, S. Schwarz, M. Sich, I. Akimov, M. Bayer, R. Schofield, E. Chekhovich, B. Robinson, N. Kay, O. Kolosov *et al.* 2D Mater. **2**, 035010 (2015).
[24] S. C. Dhanabalan, J. S. Ponraj, H. Zhang, and Q. Bao, Nanoscale **8**, 6410 (2016).
[25] H. Shangguan, L. Han, T. Zhang, R. Quhe, Q. Wang, S. Li, and P. Lu, J. Electron. Mater. **48**, 5988 (2019).
[26] J. Susoma, L. Karvonen, A. Säynätjoki, S. Mehravar, R. A. Norwood, N. Peyghambarian, K. Kieu, H. Lipsanen, and J. Riikonen, Appl. Phys. Lett. **108**, 073103 (2016).
[27] Y. Cui, D. D. Caudel, P. Bhattacharya, A. Burger, K. C. Mandal, D. Johnstone, and S. Payne, J. Appl. Phys. **105**, 053709 (2009).
[28] A. J. Nelson, A. M. Conway, B. Sturm, E. Behymer, C. Reinhardt, R. Nikolic, S. Payne, G. Pabst, and K. Mandal, J. Appl. Phys. **106**, 023717 (2009).
[29] A.-Y. Lu, H. Zhu, J. Xiao, C.-P. Chuu, Y. Han, M.-H. Chiu, C.-C. Cheng, C.-W. Yang, K.-H. Wei, Y. Yang *et al.* Nat. Nanotechnol. **12**, 744 (2017).
[30] L. Dong, J. Lou, and V. B. Shenoy, ACS Nano **11**, 8242 (2017).
[31] X. Ma, X. Wu, H. Wang, and Y. Wang, J. Mater. Chem. A **6**, 2295 (2018).
[32] Z. Guan, S. Ni, and S. Hu, J. Phys. Chem. C **122**, 6209 (2018).
[33] C. Long, Y. Dai, Z.-R. Gong, and H. Jin, Phys. Rev. B **99**, 115316 (2019).
[34] L. Zhang, Z. Yang, T. Gong, R. Pan, H. Wang, Z. Guo, H. Zhang, and X. Fu, J. Mater. Chem. A **8**, 8813 (2020).
[35] R. Li, Y. Cheng, and W. Huang, Small **14**, 1802091 (2018).
[36] H. Jin, T. Wang, Z.-R. Gong, C. Long, and Y. Dai, Nanoscale **10**, 19310 (2018).
[37] H. D. Bui, H. R. Jappor, and N. N. Hieu, Superlattices Microstruct. **125**, 1 (2019).
[38] Y. Bai, Q. Zhang, N. Xu, K. Deng, and E. Kan, Appl. Surf. Sci. **478**, 522 (2019).
[39] A. Kandemir and H. Sahin, Phys. Rev. B **97**, 155410 (2018).
[40] Y. Guo, S. Zhou, Y. Bai, and J. Zhao, Appl. Phys. Lett. **110**, 163102 (2017).
[41] P. E. Blochl, Phys. Rev. B **50**, 17953 (1994).
[42] J. P. Perdew, K. Burke, and M. Ernzerhof, Phys. Rev. Lett. **77**, 3865 (1996).
[43] G. Kresse and J. Hafner, Phys. Rev. B **47**, 558 (1993).
[44] G. Kresse and J. Furthmuller, Phys. Rev. B **54**, 11169 (1996).
[45] G. Kresse and D. Joubert, Phys. Rev. B **59**, 1758 (1999).
[46] S. Grimme, J. Comput. Chem. **27**, 1787 (2006).
[47] J. Paier, M. Marsman, K. Hummer, G. Kresse, I. C. Gerber, and J. G. Angyan, J. Chem. Phys. **124**, 154709 (2006).
[48] G. Henkelman, A. Arnaldsson, and H. Jonsson, Comput. Mater. Sci. **36**, 354 (2006).
[49] D. Alfe, Comput. Phys. Commun. **180**, 2622 (2009).
[50] A. Shafique and Y.-H. Shin, Phys. Chem. Chem. Phys. **19**, 32072 (2017).

[51] B. Liu, M. Niu, J. Fu, Z. Xi, M. Lei, and R. Quhe, Phys. Rev. Mater. **3**, 054002 (2019).

[52] See Supplemental Material at http://link.aps.org/supplemental/10.1103/PhysRevB.104.045425 for molecular dynamics simulations and dipole corrections.

[53] K.-A. N. Duerloo, M. T. Ong, and E. J. Reed, J. Phys. Chem. Lett. **3**, 2871 (2012).

[54] S. P. Poudel and S. Barraza-Lopez, Phys. Rev. B **103**, 024107 (2021).

[55] H. Wang and X. Qian, 2D Mater. **4**, 015042 (2017).

[56] T. Rangel, B. M. Fregoso, B. S. Mendoza, T. Morimoto, J. E. Moore, and J. B. Neaton, Phys. Rev. Lett. **119**, 067402 (2017).